Natural Scene-Illuminant Estimation Using the Sensor Correlation

SHOJI TOMINAGA, SENIOR MEMBER, IEEE, AND BRIAN A. WANDELL

This paper describes practical algorithms and experimental results concerning illuminant classification. Specifically, we review the sensor correlation algorithm for illuminant classification and we discuss four changes that improve the algorithm's estimation accuracy and broaden its applicability. First, we space the classification illuminants evenly along the reciprocal scale of color temperature, called "mired," rather than the original color-temperature scale. This improves the perceptual uniformity of the illuminant classification set. Second, we calculate correlation values between the image color gamut and the reference illuminant gamut, rather than between the image pixels and the illuminant gamuts. This change makes the algorithm more reliable. Third, we introduce a new image scaling operation to adjust for overall intensity differences between images. Fourth, we develop the three-dimensional classification algorithms using all three-color channels and compare this with the original two algorithms from the viewpoint of accuracy and computational efficiency. The image processing algorithms incorporating these changes are evaluated using a real image database with calibrated scene illuminants.

Keywords*—*Color balancing, color constancy, color rendering, illumination estimation, sensor correlation method.

I. INTRODUCTION

We judge the color appearance of an object using the light reflected from that object and nearby objects. The spectral composition of this reflected light, sometimes called the *color signal* depends on the surface reflectance of the objects and the spectral composition of the illuminating light. Humans have some ability to discount the illumination when judging object appearance. This ability, called *color constancy*, demonstrates at least a subconscious ability to separate the illumination spectral-power distribution from the surface reflectance function within the color signal [1].

Algorithms capable of distinguishing the surface and illuminant components have applications in several fields and illuminant estimation theory has a long history. In the fields of color science and computer vision, a large number of algorithms for separating of surface and illumination components have been proposed [2]–[25]. These algorithms can be grouped into several approaches. These include methods based on general linear models [2], [4], [7], [10], [25], reliance on highlights and mutual reflection [6], [9], [12], [14], methods based on multiband and spectral images [8], [13], [19], methods using multiple views [15]–[17], illuminant mapping approach [11], [21]–[23], and Bayesian and probabilistic approach [18], [20], [24].

These algorithms have been developed based on different motivations in various fields. In image processing, illuminant estimation algorithms are used to improve object segmentation by identifying lightness changes due to illuminant shading and highlights [26]–[31]. In color image reproduction, digital cameras often use algorithms to estimate implicitly the color of the scene illumination [32]–[35]. This estimate is used so that data acquired under one illuminant are rendered for viewing under a second illuminant [36], [37]. Finally, in image database retrieval, objects must be identified on the basis of color appearance. Estimating the perceived appearance accurately requires an estimate of the scene illuminant [38]–[41].

Nearly all illuminant estimation methods assume that there are significant physical constraints on the possible illuminant spectra, for example that a low-dimensional linear model can model the illuminants and surface reflectance functions. This assumption is necessary because accurate spectral characterization of an arbitrary illumination is impossible using an input device that obtains only three spectral samples. From a mathematical point of view, the estimation problem is underdetermined in the sense that there are more unknown scene parameters than there are available sensor data and it is nonlinear in the sense that unknown scene parameters for illuminant and surface are multiplied together to produce the values of the sensor outputs [19].

A practical factor compensates for the inescapable mathematical limits on illuminant spectral-power distribution estimation is this: in most imaging conditions the illuminant is one of several likely types, such as the variety of daylight and indoors conditions. This makes it possible to design algorithms that classify amongst possible illuminants rather than estimate from a continuous set of illuminants. Classification, rather than estimation, simplifies data processing,

Manuscript received January 5, 2001; revised September 23, 2001.

S. Tominaga is with the Department of Engineering Informatics, Osaka Electro-Communication University, Neyagawa, Osaka 572-8530, Japan (e-mail: shoji@tmlab.osakac.ac.jp).

B. A. Wandell is with the Psychology Department, Stanford University, Stanford, CA 94305 USA (e-mail: wandell@stanford.edu).

Publisher Item Identifier S 0018-9219(02)00732-6.

stabilizes computation, and is appropriate for many applications including photography [22].

In previous work [42], [43], we introduced the *sensor correlation* algorithm for classifying illuminant color temperature and we tested the method using a database of calibrated natural images. Here, we introduce changes that improve the algorithm's estimation accuracy and broaden its applicability to a variety of scenes. These improvements are confirmed using a data set of natural images measured under different illuminants. Here, we describe four main improvements that we have explored.

First, the color-temperature scale does not correspond to perceived color differences, so that estimation error does not correspond closely to perceived error [43]. To solve this problem, we describe a new method of estimating illuminant classification errors using a reciprocal color-temperature scale. The unit of this reciprocal temperature scale is the mired ($10^6 \mathrm{K}^{-1}$); a given small interval in this scale is equally perceptible, across a wide range of color temperatures. Therefore, an array of illuminant gamuts on the reciprocal color temperature is effective from the viewpoint of perceptual illuminant classification, rather than physical illuminant classification.

Second, in the original work, the pixel colors in the measured image were correlated with a reference gamut. Consequently, the resulting correlation depended on the specific pixels in the image more than their range. In some instances that we describe below, this provided unsatisfactory solutions. Here, we propose instead to compute the correlations between the gamuts of the image pixels and the illuminants. We define the image gamut as the convex hull of the set of (R, B) pixel values. The correlation is calculated between the gamuts of a given image and each of the reference illuminants gamuts. This gamut-based computation appears to make unique illuminant classification more reliable.

Third, we describe a new image scaling operation to adjust for intensity differences between images. The original sensor correlation method relies on the fact that bright image regions contain more information about the illuminant than dark regions. The dark image regions are noisy and could fall in any of the illuminant gamuts. In our original investigation on an image database, every image contained, more or less, bright neutral surfaces; illuminant information is reliable in such bright surfaces. However, if an image contains only dark chromatic surfaces, the image intensities may be scaled up excessively. Here, we describe an improved scaling operation whose performance is independent of brightness and colorfulness of the image.

Fourth, the original illuminant classification algorithms use only two of the three color channels of digital camera. This limitation is lifted at the cost of increased computation. We develop a three-dimensional (3-D) algorithm that uses all the color channels and examine its performance.

II. Illuminant Set and Color Temperature

Blackbody radiators are used frequently to approximate scene illuminants in commercial imaging and we classify

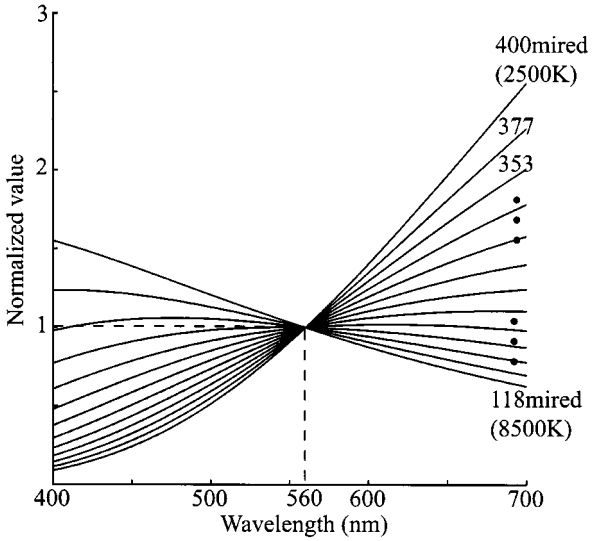

Fig. 1. Spectral power distributions of blackbody radiators.

scene illuminants according to their blackbody color temperature. The color temperature of a light source is defined as the absolute temperature (in Kelvin) of the blackbody radiator. For an arbitrary illuminant, the correlated color temperature is defined as the color temperature of the blackbody radiator that is visually closest to the illuminant. The correlated color temperature of a scene illuminant can be determined from the Commission Internationale de l'Eclairage (CIE) (x, y) chromaticity coordinates of the measured spectrum by using standard methods [44, p. 225]. A simple equation to calculate the correlated color temperature is given in [45]. The equation of the spectral radiant power of the blackbody radiators as a function of temperature T (in Kelvin) is given by the formula [44]

$$M(\lambda) = c_1 \lambda^{-5} \{\exp\left(\frac{c_2}{\lambda T}\right) - 1\}^{-1} \tag{1}$$

where $c_1 = 3.7418 \times 10^{-16}$ W/m^2 and $c_2 = 1.4388 \times 10^{-2}$ W/K and λ is wavelength (m). The spectral power distributions corresponding to color temperatures spanning 2500–8500 K are shown in Fig. 1. The set of blackbody radiators includes sources whose spectral power distributions are close to CIE standard lights commonly used in color rendering, namely, illuminant A (an incandescent lamp with 2856 K) and D_{65} (daylight with a correlated color temperature of 6504 K). Sources with lower color temperatures tend to be redder, while those with higher color temperatures are bluer.

Differences in color temperature do not correspond to equal perceptual color differences. Judd's experimental report [46] suggested that visually equally significant differences of color temperature correspond more closely to equal differences of reciprocal color temperature. The unit on the scale of microreciprocal degrees ($10^6 K^{-1}$) is called "mired." This unit is also called "remek," which is the contraction for a unit of the International System of Units (SI), the reciprocal megakelvin (MK^{-1}). Judd determined that color-temperature difference corresponding to a just noticeably different (JND) chromaticity difference over the

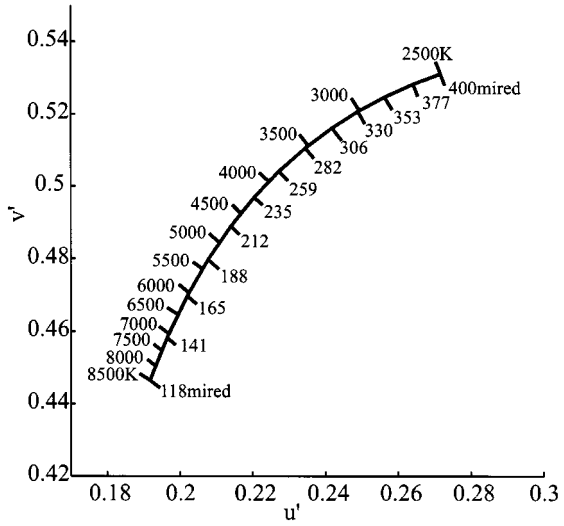

Fig. 2. Planckian locus with the scales of color temperature and reciprocal color temperature in the (u', v') chromaticity plane.

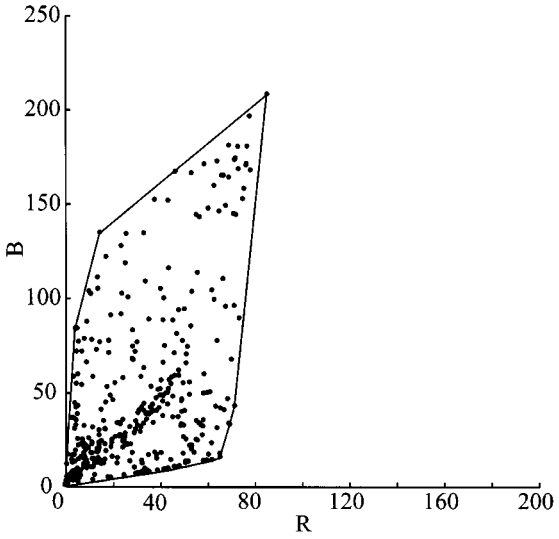

Fig. 3. Data points corresponding to the Vrhel and the Macbeth ColorChecker imaged at 182 mired (5500 K) are superimposed on the RB sensor plane.

range of 1800–11 000 K. Let dE be the JND chromaticity difference corresponding to the color-temperature difference dT. He derived the JND color temperature of the ratio dT/dE as a function of color temperature by the empirical relation

$$\frac{dT}{dE} = 5.5T^2 \times 10^{-6}. \tag{2}$$

This difference is represented by reciprocal color temperature $T'(= 10^{6/T})$ as

$$\frac{dT'}{dE} = 10^6 \frac{d\left(\frac{1}{T}\right)}{dE} = -5.5. \tag{3}$$

This result means that a just noticeable difference in reciprocal color temperature is 5.5 mired. The blackbody radiators are written as a function of reciprocal temperature T' as

$$M(\lambda) = c_1 \lambda^{-5} \{\exp\left(\frac{c_2 T'}{\lambda}\right) - 1\}^{-1} \tag{4}$$

where $c_1 = 3.7418 \times 10^{-16}$ W/m^2 and $c_2 = 1.4388 \times 10^4$ W/mired. In Fig. 1, the spectral-power distributions of the blackbody radiators are represented at the reciprocal color temperatures, spanning $T'(1) = 118$ mired (8500 K) to $T'(13) = 400$ mired (2500 K) in 23.5 mired increments. These numbers are 117.65, 400.00, and 23.529 in the five significant digits. Fig. 2 shows the Planckian locus (chromaticity locus of blackbody radiators) in the (u', v') plane of the CIE 1976 UCS chromaticity diagram, where the locus is segmented in two ways of equal color-temperature steps and equal reciprocal color-temperature steps. Note that small intervals in reciprocal color temperature are more nearly perceptually equal than small intervals in color temperature.

III. Definition of Illuminant Gamuts

Illuminant classification algorithms use a set of reference illuminant gamuts to define the anticipated range of sensor responses. To create these gamuts, we used a database of surface-spectral reflectances provided by Vrhel *et al.* [47] together with the reflectances of the Macbeth ColorChecker. The image data were obtained using a Minolta camera (RD-175) with known sensor responsivities. Hence, the sensor responses can be predicted using

$$\begin{bmatrix} R \\ G \\ B \end{bmatrix} = \int_{400}^{700} S(\lambda) M(\lambda) \begin{bmatrix} r(\lambda) \\ g(\lambda) \\ b(\lambda) \end{bmatrix} d\lambda \tag{5}$$

where $S(\lambda)$ is the surface-spectral reflectance function, $r(\lambda)$, $g(\lambda)$, and $b(\lambda)$ are the spectral responsivities, and $M(\lambda)$ is the scene illuminant. The Minolta camera can be operated in one of two modes. In one mode, appropriate for imaging under tungsten illumination (say, illuminant A), the blue sensor gain is high. In a second mode, appropriate for imaging under daylight (D65), the blue sensor gain is much lower. Operating in the high blue sensor gain improves the performance of the scene-illuminant classification. Hence, all analyses throughout this paper were performed in this mode. The example images shown in figures below have been color balanced only for display purposes. The scene illuminants for classification are blackbody radiators spanning 118 mired (8500 K) to 400 mired (2500 K) in 23.5-mired increments, as shown in Fig. 1.

The illuminant gamuts are defined on the RB plane. This sensor plane is a reasonable choice for the blackbody radiators because the illuminant gamuts differ mainly with respect to this plane. The boundary of the illuminant gamut is obtained from the convex hull of the set of (R, B) points. For example, Fig. 3 shows the set of data points corresponding to the Vrhel and the Macbeth ColorChecker superimposed on the illuminant gamut for the particular temperature of 182 mired (5500 K). The region enclosed with the solid curves represents the illuminant gamut. Fig. 4 shows the illuminant gamuts of the blackbody radiators for 13 successive temperatures in the RB plane in two ways. In Fig. 4(a), gamuts are depicted at equal spacing in reciprocal color temperatures, while in Fig. 4(b), gamuts are depicted

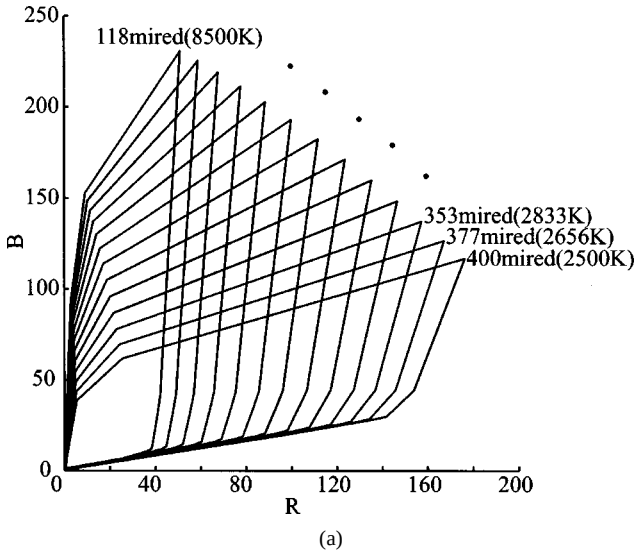

(a)

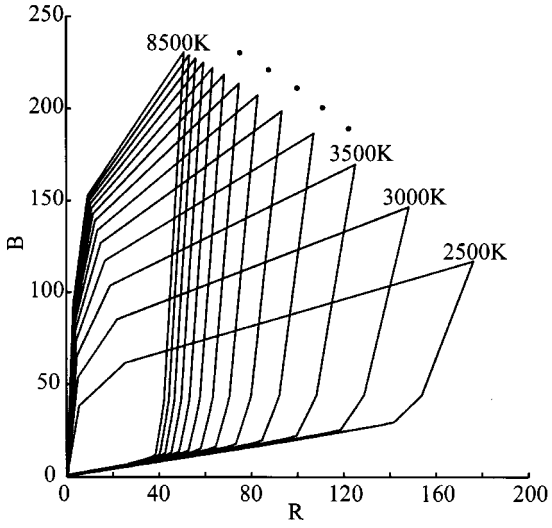

(b)

Fig. 4. Illuminant gamuts for blackbody radiators for 13 successive temperatures in the RB sensor space. Gamuts are depicted at equal spacing in (a) reciprocal color temperatures and (b) color temperatures.

in equal spacing of color temperatures, spanning from 2500 K to 8500 K in 500 K increments. Note that 13 gamuts are arranged in the same temperature range [2500, 8500 K] in both figures. The illuminant gamuts separated by equal reciprocal color- temperature steps are better separated than those separated in equal color-temperature steps.

Experimentally, we have found that many cameras exhibit the same good spacing in the RB plane as shown in Fig. 4(a). We use 23.5-mired increments to have the same number of gamuts in the common range [2500, 8500 K] as we used in previous work [42], [43]. In this way, we can compare the performance of illuminant classification between the two scale systems.

A gamut correlation coefficient is a useful figure of merit to evaluate the ability of different gamut classes to separate illuminants. The gamut correlation coefficient can be computed between a pair of illuminant gamuts using the formula

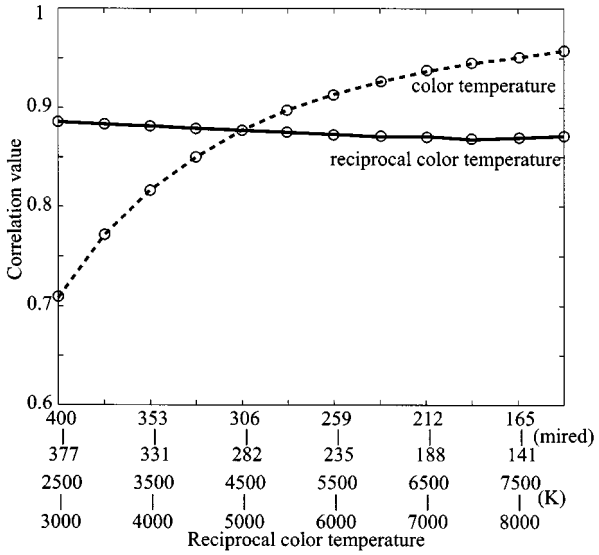

Fig. 5. Gamut correlation coefficients between adjacent illuminant gamuts. Correlation is approximately constant in mired steps, but not color-temperature steps.

$c_{ij} = G_{ij}/\sqrt{G_i G_j}$, where G_i and G_j are the areas of ith and jth gamuts and G_{ij} is the area of overlap between two gamuts. Fig. 5 shows the gamut correlation coefficients between adjacent gamuts measured with equal color-temperature spacing and equal mired spacing. The constant correlation level in mired confirms that the gamuts in reciprocal color temperature are uniformly separated.

IV. Computational Methods

A. Pixel-Based Illuminant Classification

The original sensor correlation illuminant classification algorithm uses a correlation between image data and illuminant gamuts. The RB plane is divided into a regular grid (i, j) with small equal-sized intervals (usually 256×256 points). The illuminant gamuts are represented by setting a $g(i, j)$ value 1 or 0, depending on whether or not the cell falls inside the convex hull. Image data are mapped into an array of cells with the same size as $g(i, j)$, essentially converting the image to a two-dimensional (2-D) binary map (with possible holes). The correlation between an image and each of the illuminant gamuts can be computed by simply summing the binary values on the gamut array $g(i, j)$ corresponding to the (R, B) pixel values of the image RGB. This correlation is a very quick binary computation without multiplication or conditional statements. A program for an efficient correlation computation is provided in [43].

We can demonstrate the method using a simulation based on the Macbeth ColorChecker. First, we measured the surface-spectral reflectances for 24 color patches of the Macbeth ColorChecker. The image data at 182 mired (5500 K) were calculated from (5) with the measured reflectances and the blackbody radiator. Then, Gaussian random numbers with the mean of zero and the standard deviation of 1% were added to the RGB values to simulate observational noise. Fig. 6(a) shows the synthesized image of the Macbeth

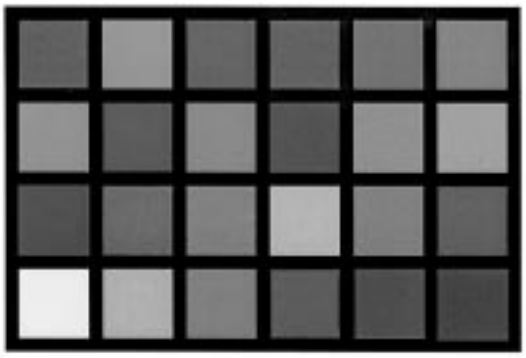

(a)

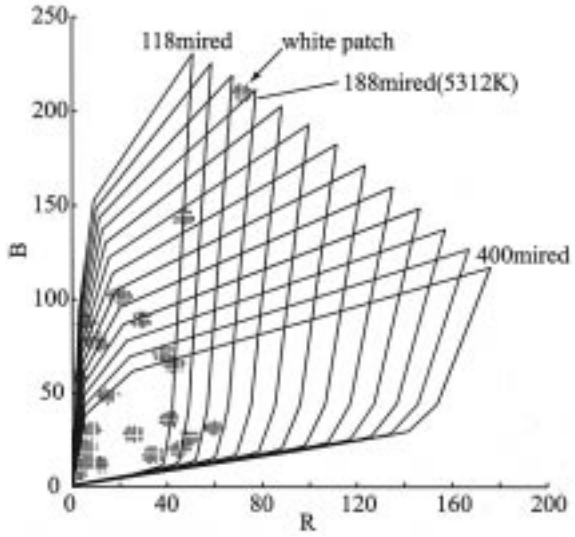

(b)

Fig. 6. (a) Synthesized image of the Macbeth ColorChecker at 5500 K. (b) Plot of the (R, B) pixel values on the gamuts.

ColorChecker at 182 mired (5500 K). Fig. 6(b) shows (R, B) pixel values superimposed on the illuminant gamuts. In the figure, the data points vary slightly because of the added noise. The large sensor values, which fit selectively the gamut near 188 mired, fall outside all of the illuminant gamut classes and, thus, do not contribute to the pixel-based correlation for any illuminant gamut $T'(i)$, $i = 1, \ldots, 13$. Fig. 7 shows the correlation function between the image pixels and each of the illuminant gamuts. The peak correlation is at a reciprocal temperature of 188 mired (5312 K), which is selected as the estimate.

This pixel-based correlation depends greatly on the specific color elements of an image and not on their range: changing the position of image data points within a reference gamut does not change the correlation value. This can pose a problem when there are only a few color samples are sparsely scattered in the RB plane and the binary histogram of (R, B) pixel values has many holes. This is illustrated by Fig. 8(a), which shows the synthesized image consisting of 18 chromatic patches of the Macbeth ColorChecker; for this example the achromatic patches have been removed (cf. Fig. 6). Fig. 8(b) shows the (R, B) pixel values on the gamut, where the maximal value of the intensity over the image is

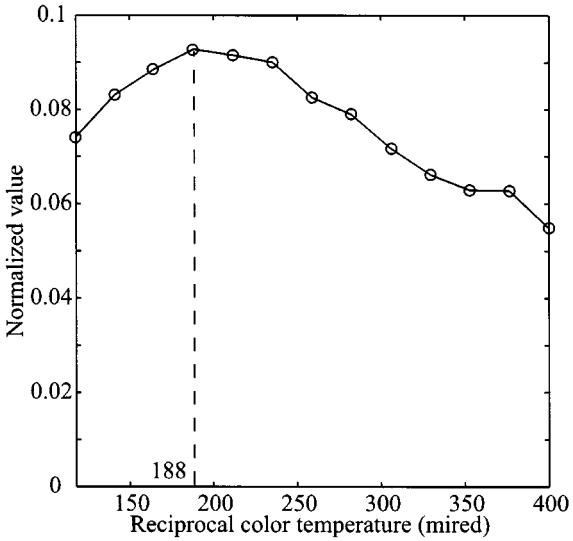

Fig. 7. Correlation function between image pixels and illuminant gamuts for the synthesized Macbeth image.

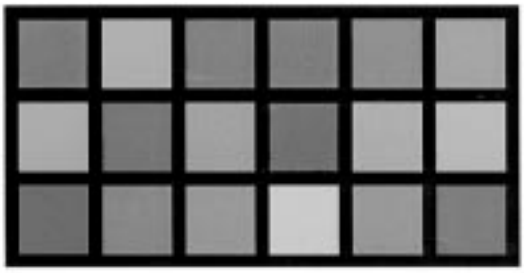

(a)

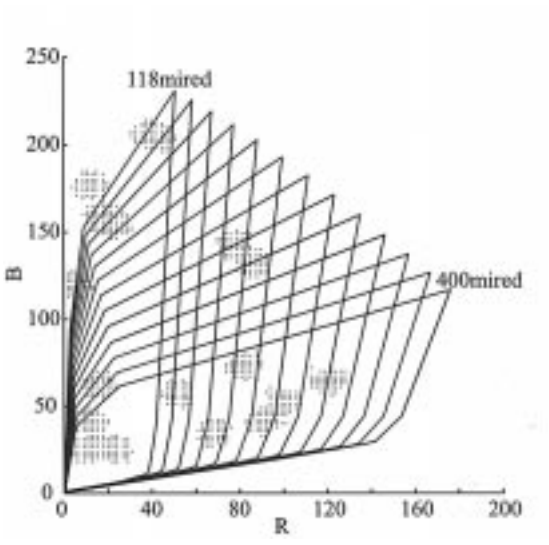

(b)

Fig. 8. (a) Synthesized image of the chromatic color patches for the Macbeth image. (b) Plot of the (R, B) pixel values on the gamuts.

normalized to 255. The clusters of pixels for chromatic color patches are distributed in the RB plane in a way that makes selecting the proper gamut very difficult.

This visual impression from Fig. 8 is confirmed by the correlation function in Fig. 9. The maximum correlation should

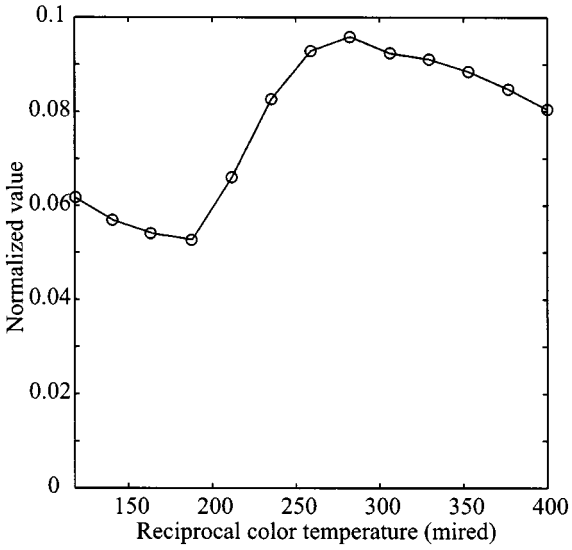

Fig. 9. Correlation function between image pixels and reference illuminant gamuts for Fig. 8.

occur when all image pixels fall in the corresponding illuminant gamut and the correlation should decrease as the gamut color temperature differs from the real temperature. However, an image comprising only the chromatic patches has very poor properties for the original illuminant classification algorithm. Furthermore, we repeated the above simulation experiment at different noise levels. The peak of the correlation function fluctuated varies significantly with noise in these cases.

B. Gamut-Based Illuminant Classification

1) Image Gamut: To reduce the problem caused by sparse histograms, we propose using the convex hull of the image data, rather than the data themselves, to determine an image gamut in the RB plane. In this modified calculation we compute the correlation value between the image and illuminant gamuts.

The image gamut defines an entire region of possible colors in the RB plane, which is predicted from the observed image data under a certain illuminant. Because the convex hull is the smallest convex set of pixel values, the extreme colors, such as the brightest colors and the most saturated colors in the observed image, define the image gamut [11]. In fact, since a set of the brightest and the most saturated colors approximates the convex hull of image pixels, the extreme colors that define the range of the data are the most important data for specifying the image gamut. The interior points are irrelevant to the image gamut; even if some interior colors are deleted or new colors are added to the inside, the corresponding illuminant gamut is unchanged [11].

Theoretically, the interior points of the image convex hull might be considered as implicit image data. To see why, consider the image gamut shown in Fig. 10. Five points $\mathbf{C}_1, \mathbf{C}_2, \ldots, \mathbf{C}_5$ form the convex hull defining the image gamut on the RB plane; the interior points can be viewed as additive mixtures of these points. Now, suppose that two points $\mathbf{C}_1$ and $\mathbf{C}_2$ are associated with surface reflectance

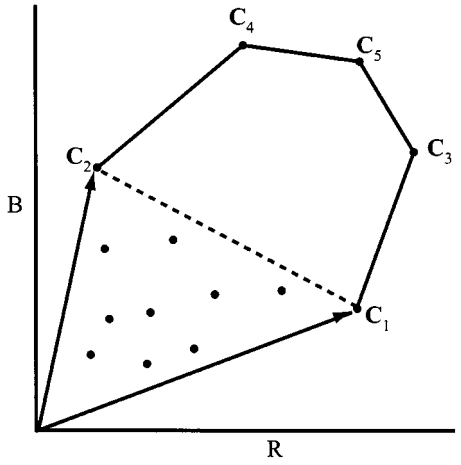

Fig. 10. Relationship between image pixels and the image gamut.

functions S_1 and S_2. The interior points along the line connecting these points could arise from a surface with reflectance

$$\begin{aligned}\mathbf{C} &= \mathbf{C}_1 + \mathbf{C}_2 \\ &= \int_{400}^{700} \left(w_1 S_1(\lambda) + w_2 S_2(\lambda)\right) M(\lambda) \begin{bmatrix} r(\lambda) \\ g(\lambda) \\ b(\lambda) \end{bmatrix} d\lambda \quad (6)\end{aligned}$$

where w_1 and w_2 are weights with constraints $0 < w_1, w_2 \leq 1$.

Finite-dimensional linear models are frequently used to describe the set of possible reflectance functions

$$S(\lambda) = \sum_{i=1}^{n} \sigma_i S_i(\lambda) \quad (7)$$

where $\{S_i(\lambda),\ i = 1,\ 2,\ \ldots,\ n\}$ is a set of basis functions for reflectance and $\{\sigma_i\}$ is a set of weighting coefficients. Hence, it is likely that these interior points are present within the linear model of surface reflectance approximations, even if that point is not present in the image itself.

The gamut-based correlation differs from the pixel-based correlation in that the calculation presumes that interior points might all have been present in the scene. A practical correlation value is computed from the area of the gamuts as

$$r_i = \frac{A_{Ii}}{\sqrt{A_I A_i}}, (i = 1, 2, \ldots, 13) \quad (8)$$

where A_I is the area of an image gamut, A_i are the area of the ith illuminant gamut, and A_{Ii} is the area of the overlap between the image and illuminant gamuts.

Figs. 11 and 12 illustrate the improvement we have observed with the gamut-based correlation. Fig. 11 shows the gamut for the image shown in Fig. 8, where the solid curve represents the convex hull of (R, B) values and the region surrounded by this curve represents the image gamut. Fig. 12 shows the correlation function between the image gamut and each of the illuminant gamuts. The function clearly indicates a unique illuminant, unlike the pixel-based function in Fig. 9. The peak correlation indicates an illuminant of 235 mired (4249 K). The gamut-based classification is stable although it

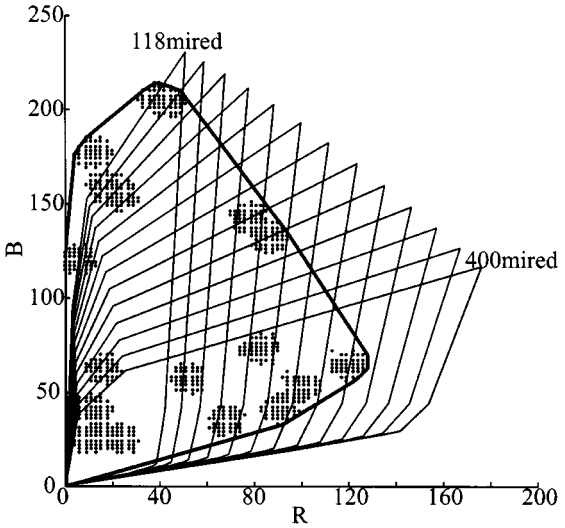

Fig. 11. Convex hull of (R, B) values and image gamut for the image of chromatic patches in Fig. 8.

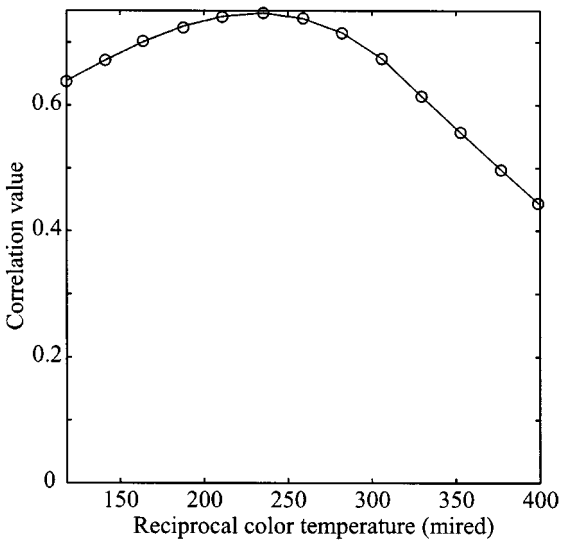

Fig. 12. Correlation function between the image gamut and each of the illuminant gamuts for Fig. 8.

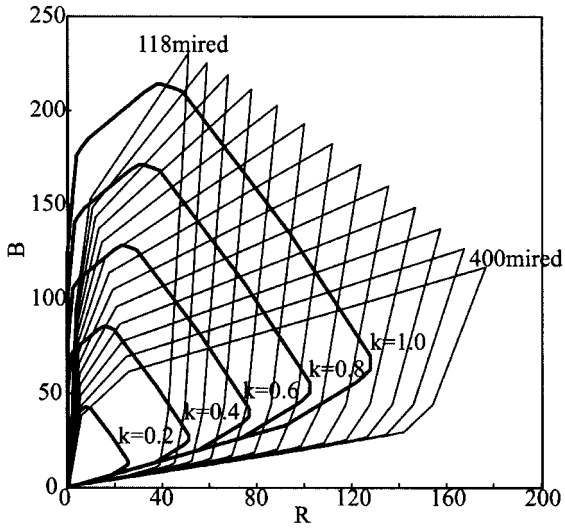

Fig. 13. Convex hulls of the scaled (R, B) values with different normalization parameter k levels.

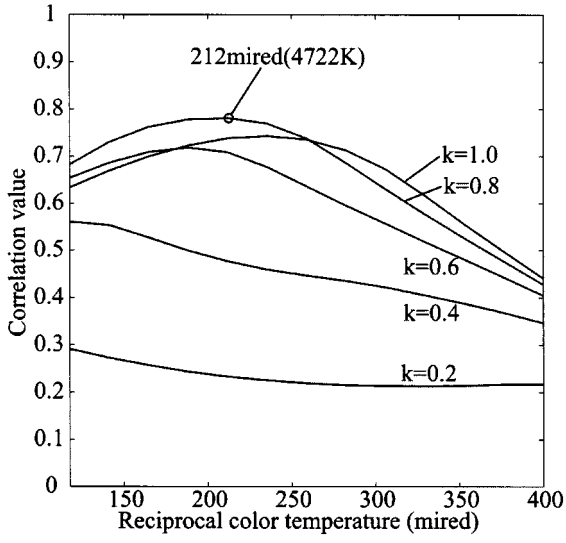

Fig. 14. Correlation functions for different normalization parameter levels.

is computationally more expensive than the pixel-based classification.

2) Image Scaling: The sensor correlation method requires a scaling operation that compensates for intensity differences between images. This scaling operation is equivalent to placing a neutral density filter in the light path or adjusting the exposure duration. Scaling preserves the shape of the image gamut and the relative intensity information within an image. To scale the data, we define I_i as the ith pixel intensity

$$I_i = \left(R_i^2 + G_i^2 + B_i^2\right)^{1/2} \tag{9}$$

and let $I_{\max}$ be the maximal value of the intensity over the image. Then, to scale the intensity across different images, we divide the sensor RGB values by the maximum intensity

$$(R, G, B) = \left(\frac{R}{I_{\max}}, \frac{G}{I_{\max}}, \frac{B}{I_{\max}}\right). \tag{10}$$

Bright image regions contribute much of the illuminant information. This is especially true if nearly white surfaces are present in the scene in which case these image regions mainly determine the color-temperature estimate. However, if there is no bright surface, the scaling operation converts dark surfaces into bright image regions and the estimation accuracy decreases. Hence, the selection of a proper scaling parameter is an important element of the algorithm.

In the initial formulation of the sensor correlation algorithm, we chose the scaling parameter based on a set of properties of the brightest pixels. Since then, we have discovered a better normalization method that is illustrated in Figs. 13 and 14. Fig. 13 shows the convex hulls of the (R, B) pixel values of the image in Fig. 8. These convex hulls are each scaled by a different normalization parameter k. A set of these image gamuts were used to generate the correlation functions shown in Fig. 14; each curve shows the function for a different parameter k. To select a value k, we compute

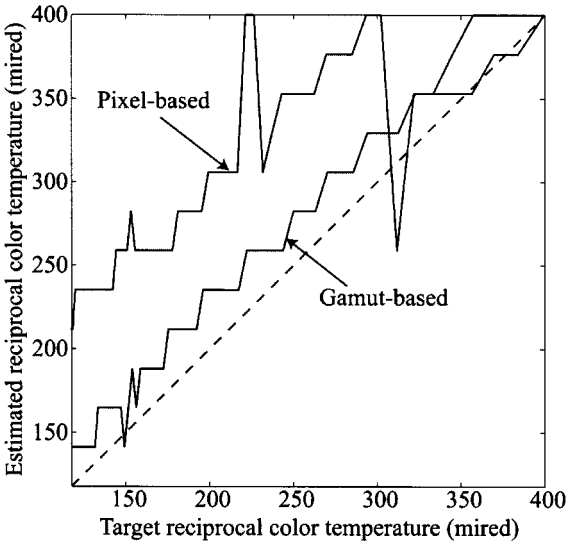

Fig. 15. Illuminant classification comparisons of the pixel- and gamut-based methods.

all of these gamuts and then choose the peak correlation over all the functions. In this example, the peak correlation occurs for $k = 0.8$ and a reciprocal color temperature of 212 mired (4722 K). This normalization procedure, which we apply to the gamut, can also be applied to the image data [23].

To investigate the overall performance of the gamut-based illuminant classification, we performed a computer experiment. Using 18 chromatic patches of the Macbeth ColorChecker, we generated 61 images under different illuminants by changing the color temperatures from 2500 K to 8500 K in 100 K increments. Fig. 15 compares the illuminant classification results using the pixel- and gamut-based classification methods. The horizontal axis represents the target color temperature (mired) and the vertical axis represents the estimate. A perfect classifier without error represents a staircase version of the broken line. The stair step error is due to the sampling every 23.5 mired. Therefore, the finer sampling becomes the smaller error. The property of consistent bias is just a function of the Macbeth color samples. The estimates are not biased for all images. In this experiment, a yellow patch in the Macbeth samples affects strongly the bias of the estimates. It is clear that the gamut-based classification method outperforms the pixel-based method.

C. Three-Dimensional Illuminant Classification

The original sensor correlation method uses only two of the three color channels. This limitation can be lifted at the cost of increased computation. Fig. 16 shows a collection of the 3-D illuminant gamuts in an RGB sensor space. These gamuts are obtained from the convex hull of the set of (R, G, B) points calculated using the reflectance database and the blackbody radiator from 118 mired (8500 K) to 400 mired (2500 K) in 23.5 increments. The illuminant gamuts differ only a little with respect to the G axis. Moreover, the gamuts move monotonically as R or B increases, but they do not move monotonically as G increases. Mathematically, the gamuts are a type of two-valued function with respect to G.

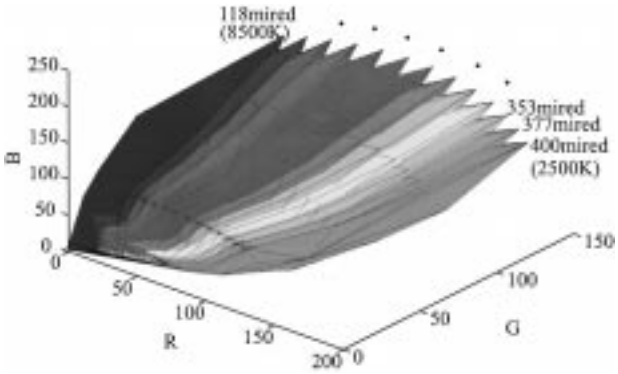

Fig. 16. 3-D illuminant gamuts in RGB sensor space.

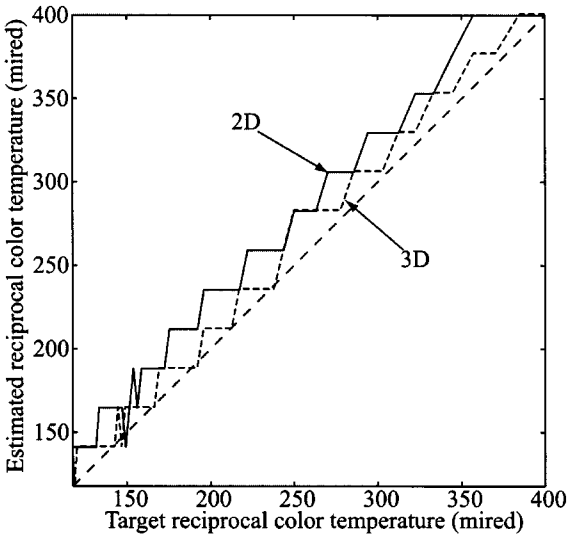

Fig. 17. Illuminant classification comparison of the 2-D and 3-D gamut-based algorithms.

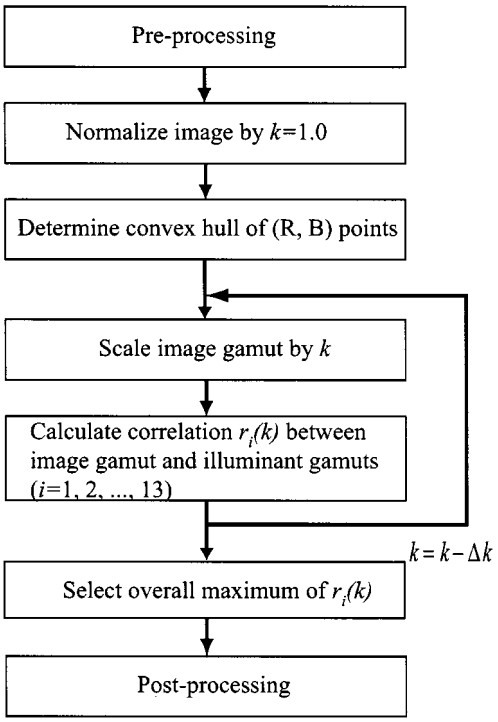

Fig. 18. Algorithm flow for the gamut-based illuminant classification.

(a)

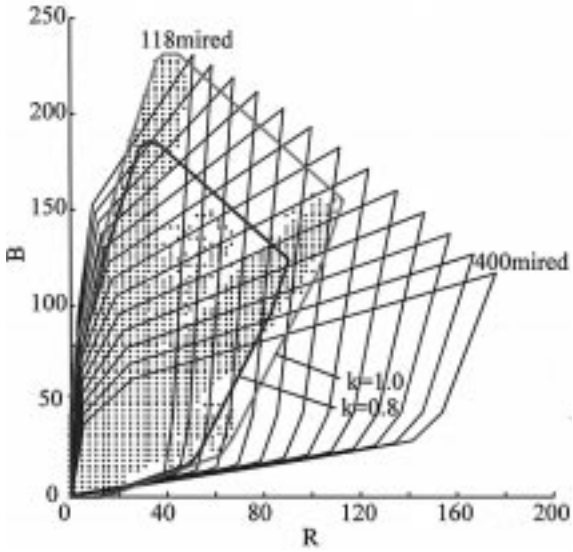

(b)

Fig. 19. (a) Image acquired outdoors under a daylight. (b) Pixel distribution with illuminant gamut.

Moreover, the gamut size varies with color temperature. Inspecting the projected GR gamuts, we found that the 118-mired gamut contains most of the other gamuts and there is little separation between gamuts at high color temperature of blue region. Hence, the inclusion of G channel does not lead to significantly better classification.

In order to evaluate the 3-D classification algorithm, a computer experiment was performed using 61 images of 18 chromatic patches of the Macbeth ColorChecker at different color temperatures from 2500 K to 8500 K in 100 K increments. Two types of 2-D and 3-D gamuts were used for illuminant classification. Fig. 17 shows the classification results based on the 2-D and 3-D gamut-based classification algorithms. The 45° line represents perfect classification. The 3-D algorithm estimates are closer to the exact temperatures than the 2-D algorithm estimates. However, the computation time of the 3-D algorithm is 30 times that of the 2-D algorithm, mainly due to the long time required to calculate the 3-D convex hull. Therefore we have decided that the 2-D algorithm is effective from the overall viewpoint of accuracy and computation.

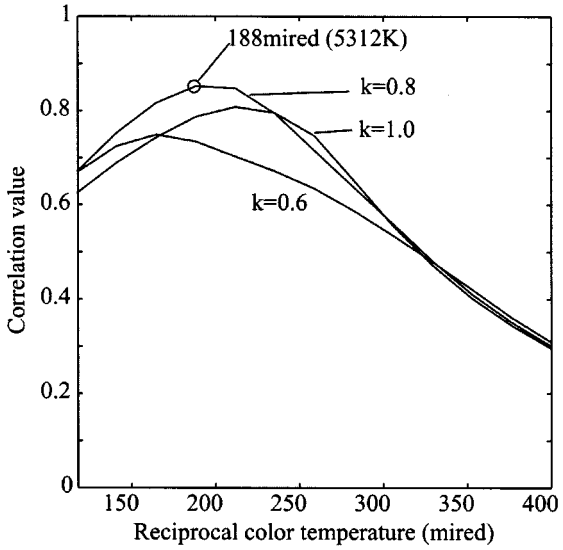

Fig. 20. Correlation functions for Fig. 19.

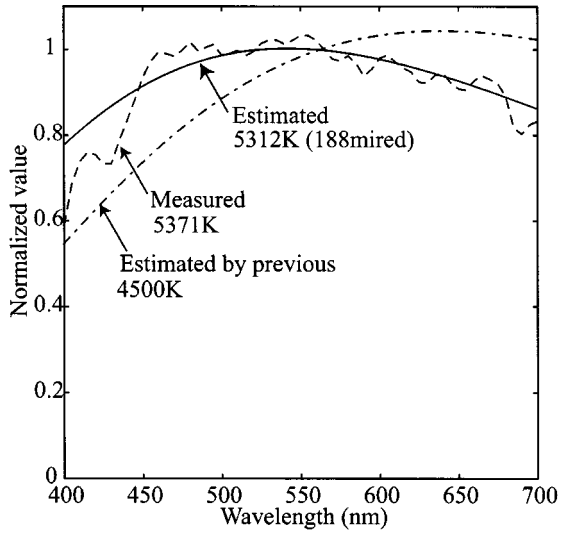

Fig. 21. Estimation results of the scene-illuminant spectrum. Solid curve represents the estimated spectral distribution of the blackbody radiator, the dashed curve represents the measured illuminant, and the short-long dashed curve represents the estimate by the previous method in [43].

D. Image Processing

Fig. 18 illustrates the algorithm flow for the gamut-based illuminant classification. First, in the preprocessing step, illuminant gamuts of blackbody radiators from 118 to 400 mired in 23.5-mired increments are created. Also, the convex hull of the image (R, B) values is determined. It is important that this gamut be stable with respect to various noise effects such as those that might be caused by a single bad pixel. To insure this stability, we perform some simple preprocessing.

First, to guarantee that the image gamut is reliable, we remove noisy pixels during the preprocessing by identifying isolated pixels in the (R, G, B) volume. Let (R_0, G_0, B_0) be the color point of a pixel. We investigate connectivity of (R_0, G_0, B_0) to 26 nearest neighbors at coordinates $(R_0 - 1, G_0 - 1, B_0 - 1), \ldots, (R_0 + 1, G_0 + 1, B_0 + 1)$ excluding (R_0, G_0, B_0) itself. If the point (R_0, G_0, B_0) has no or only

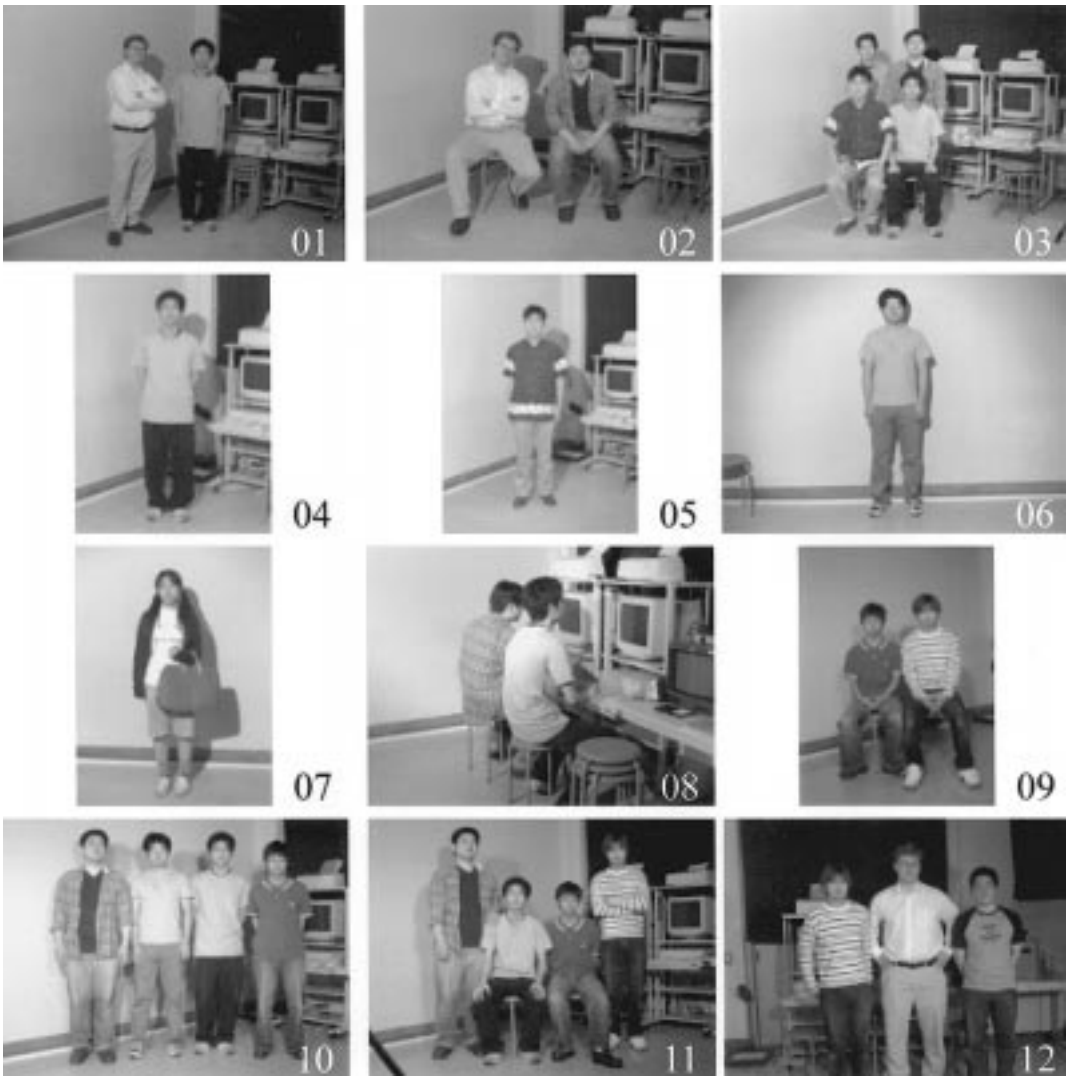

Fig. 22. Set of images of indoor scenes under a halogen lamp.

one connection to its neighbors, the pixel is identified as isolated and it is excluded.

Second, we exclude saturated pixels in the original image. Ideally, if a pixel has one value of RGB equal to 255, it should be thrown out as a saturated pixel. Actually, pixels with values ≥ 225 are regarded as saturated in the present camera system.

Following this preprocessing, the entire image is normalized so that the brightest pixel has the maximum intensity 255. The convex hull of these normalized values is determined on the RB plane. Once the original image gamut is fixed, the correlation computation is repeated between the image gamut, scaled with a different value of the parameter k and illuminant gamuts ($i = 1, 2, \ldots, 13$). It is not necessary to repeat the image normalization or the determination of the corresponding convex hull with different k values.

Finally, we determine the illuminant $i_{\max}$ and the parameter $k_{\max}$, which give an overall maximum of the correlation function. The scene illuminant is classified to be a blackbody radiator within a temperature interval of 23.5 mired. The value of $\Delta k = 0.1$ is the most suitable for selecting one gamut from 13 illuminant gamuts. As the number of gamuts increases, a smaller value of Δk should be used.

V. Experimental Results

We have evaluated the proposed algorithm using a database of images that include both indoor and outdoor scenes [48]. As an example, the gamut-based illuminant classification algorithm is applied to the image in Fig. 19(a). This image was acquired outdoors under daylight with correlated color emperature of 5371 K. The scaled (R, B) values are plotted in Fig. 19(b), where the image gamuts are depicted for two scale factors $k = 0.8$ and $k = 1.0$. Fig. 20 shows the correlation functions between the image gamuts for $k = 0.6, 0.8, 1.0$ and the illuminant gamuts in the interval of 23.5 mired. Comparing across categories and scale factor levels, the overall peak correlation is at a color temperature of 188 mired (5312 K) for $k = 0.8$. The difference from the measurement is 2.1 mired. The solid curve in Fig. 21 represents

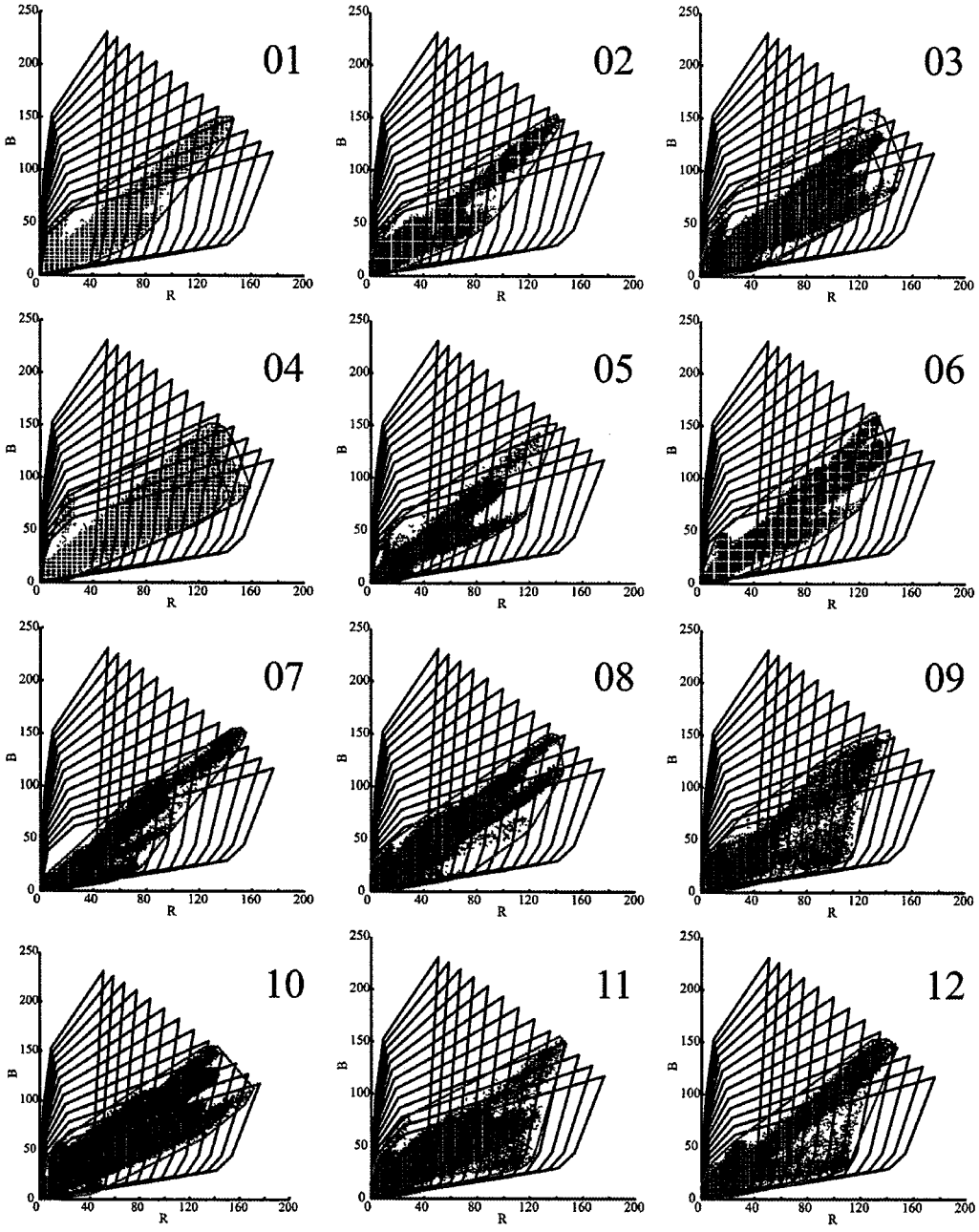

Fig. 23. Pixel distributions and image gamuts for the indoor images.

the estimated spectral distribution of the blackbody radiator. The dashed curve shows the spectral-power distribution of a direct spectroradiometric measurement made by placing a reference white in the scene; there is a good agreement between the estimate and the measurement. The accuracy is better than that of the original sensor correlation method (short–long dashed curve), which has an estimated temperature of 4500 K and an error of 36 mired.

Fig. 22 shows a set of 12 images of scenes photographed under a halogen lamp in our laboratory. This illuminant has a correlated color temperature near 3100 K. Fig. 23 depicts a whole set of the pixel distributions and the image gamuts. The numerical results of illuminant classification are listed in Table 1. The estimate of scene illuminant is expressed in the color-temperature unit (Kelvin) and the difference between

Table 1
Illuminant Classification Results for the Indoor Images

No.	Measured (K)	Proposed method		Previous method	
		Estimate (K)	Difference (mired)	Estimate (K)	Difference (mired)
1	3103	3035	7.2	3000	11.1
2	3103	3035	7.2	3000	11.1
3	3103	3035	7.2	3000	11.1
4	3103	3035	7.2	3000	11.1
5	3103	3269	16.4	3000	11.1
6	3106	3035	7.5	3000	11.4
7	3106	3035	7.5	3000	11.4
8	3083	3035	5.1	3000	9.0
9	3062	3035	2.9	3000	6.7
10	3062	3035	2.9	3000	6.7
11	3062	3035	2.9	3000	6.7
12	3045	3035	1.1	3000	4.9

Fig. 24. Outdoor scenes in Kyoto used in the database.

the estimate by the image and the direct measurement by the spectroradiometer is expressed in the reciprocal color-temperature unit (mired). The proposed modifications improve the estimates for all images except image 5, where bright texture on the shirt has random fluctuations of pixels. The difference between estimates and direct measurement is 6.3 mired on average, while the difference for the original method is 9.4 mired.

Fig. 24 shows a set of images acquired in Kyoto in spring. The pixel distributions and the illuminant gamuts are depicted in Fig. 25. Most of the pixel distributions of the outdoor scenes form linear clusters in the RB plane, so that the convex hulls fit the respective pixel distributions well compared to the indoor scenes in Fig. 23. The numerical classification results are shown in Table 2. The direct measurements of color temperature in outdoor scenes vary over time and with the viewing direction. The measurements for the scenes in Kyoto ranged widely from 4843 to 6038 K. The color-temperature estimates of the scene illuminants differ by only 4.7 mired.

The spectral distribution error of the illuminant can be expressed as CIELAB color difference with respect to the average surface (see [43] for the details). The average errors for the proposed method are $\Delta E_{ab} = 4.04$ for the

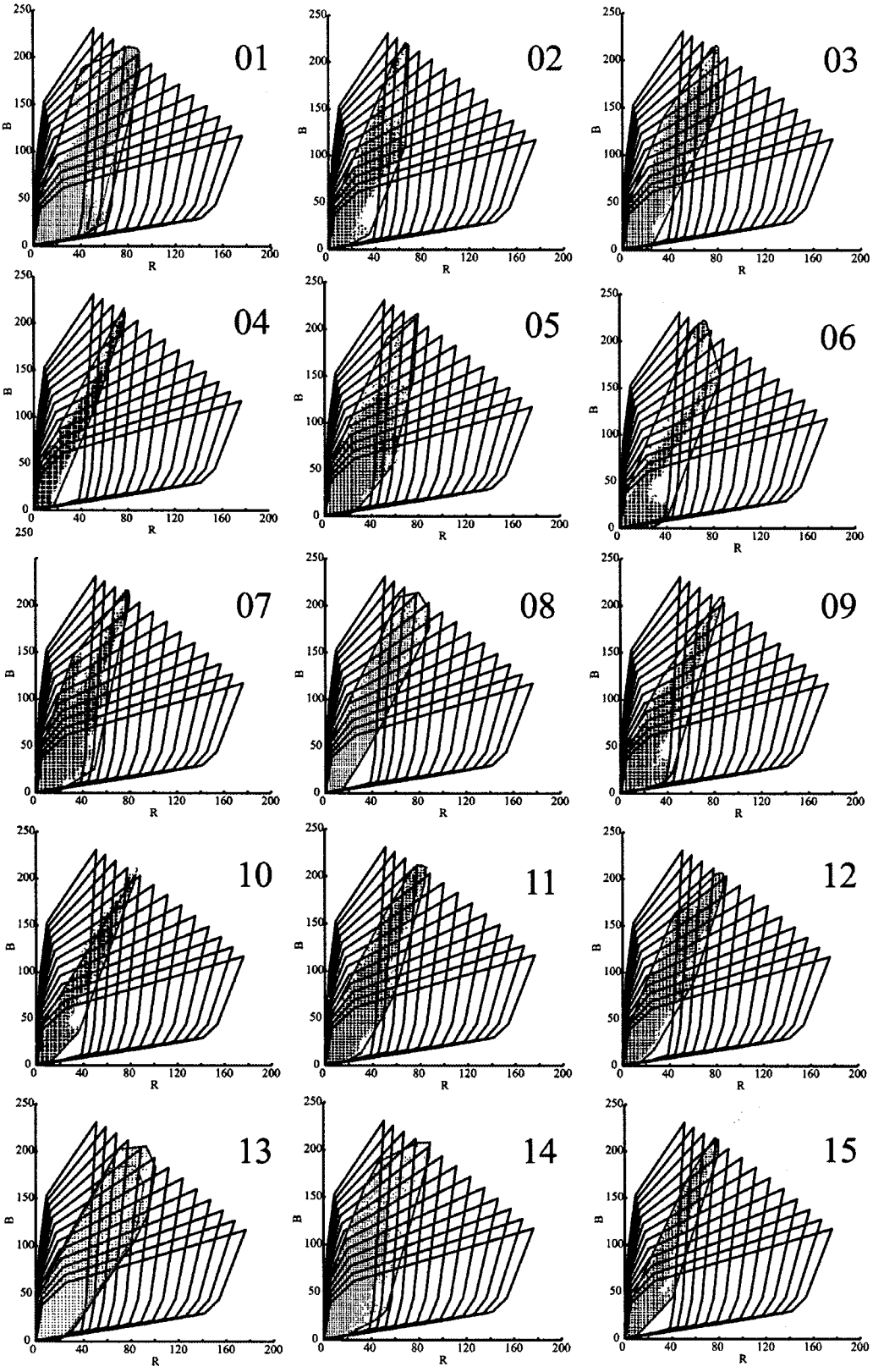

Fig. 25. Pixel distributions and image gamuts for the outdoor images.

indoor scenes and $\Delta E_{ab} = 3.02$ for the outdoors scenes. Finally, the performance was compared with a classical algorithm based on the gray-world assumption. In this case, the averages of the RGB sensor values for the entire image were used for illuminant classification. The color-temperature estimation error increased from less than 5 mired to 11.3 mired for the indoor scenes and 32.2 mired for the outdoors scenes.

Table 2
Illuminant Classification Results for the Outdoor Images

No.	Measured (K)	Proposed method		Previous method	
		Estimate (K)	Difference (mired)	Estimate (K)	Difference (mired)
1	5687	5312	12.4	5000	24.2
2	6038	6071	0.9	6000	1.0
3	5428	5312	4.0	5000	15.8
4	5361	5312	1.7	5000	13.5
5	5222	5312	3.2	5500	9.7
6	5646	5312	11.1	5000	22.9
7	5160	5312	5.5	5000	6.2
8	5479	5312	5.7	5000	17.5
9	5206	5312	3.8	5000	7.9
10	5239	5312	2.6	5000	9.1
11	5226	5312	3.1	5000	8.6
12	5194	5312	4.3	5000	7.5
13	4843	4722	5.3	4500	15.7
14	5410	5312	3.4	5000	15.2
15	5397	5312	3.0	5500	3.5

VI. Conclusion

We have described extensions of the sensor correlation method for illuminant classification and discussed several methods that improve the accuracy and scope of the algorithm. First, the reciprocal scale of color temperature should be used to achieve perceptually uniform illuminant classification. Second, we proposed that a gamut-based correlation value should be calculated between an image gamut and the reference illuminant gamuts in order to use the most relevant information when selecting an illuminant. Third, we have proposed a new normalization operation that makes classification performance independent of image intensity. Fourth, we have developed the 3-D classification algorithms using all three-color channels. The first three changes all improve algorithm performance. The comparison of the 2-D and 3-D algorithms shows little improvement in accuracy, so that for efficiency we believe the 2-D algorithms are more effective. Finally, the applicability of the improved algorithm was shown using an expanded database of real images.

Acknowledgment

The authors would like to thank A. Ishida for his help in experiments and data processing.

References

[1] B. A. Wandell, *Foundations of Vision*. Sunderland, MA: Sinauer, 1995.
[2] G. Buchsbaum, "A spatial processor model for object color perception," *J. Franklin Inst.*, vol. 310, pp. 1–26, 1980.
[3] M. H. Brill and G. West, "Contributions to the theory of invariance of color under the condition of varying illumination," *J. Math. Biol.*, vol. 11, pp. 337–350, 1981.
[4] L. T. Maloney and B. A. Wandell, "Color constancy: A method for recovering surface spectral reflectance," *J. Opt. Soc. Amer. A*, vol. 3, no. 1, pp. 29–33, Jan. 1986.
[5] M. D'Zmura and P. Lennie, "Mechanisms of color constancy," *J. Opt. Soc. Amer. A*, vol. 3, no. 10, pp. 1662–1682, Oct. 1986.
[6] H. C. Lee, "Method for computing the scene-illuminant chromaticity from specular highlights," *J. Opt. Soc. Amer. A*, vol. 3, no. 10, pp. 1694–1699, Oct. 1986.
[7] B. A. Wandell, "The synthesis and analysis of color images," *IEEE Trans. Pattern Anal. Machine Intell.*, vol. PAMI-9, pp. 2–13, Jan. 1987.
[8] S. Tominaga and B. A. Wandell, "The standard surface reflectance model and illuminant estimation," *J. Opt. Socer. Amer. A*, vol. 6, no. 4, pp. 576–584, Apr. 1989.
[9] G. J. Klinker, S. A. Shafer, and T. Kanade, "A physical approach to color image understanding," *Int. J. Comput. Vision*, vol. 4, no. 1, pp. 7–38, 1990.
[10] J. Ho, B. V. Funt, and M. S. Drew, "Separating a color signal into illumination and surface reflectance components: Theory and applications," *IEEE Trans. Pattern Anal. Machine Intell.*, vol. 12, pp. 966–977, Oct. 1990.
[11] D. A. Forsyth, "A novel algorithm for color constancy," *Int. J. Comput. Vision*, vol. 5, no. 1, pp. 5–36, 1990.
[12] G. Healey, "Estimating spectral reflectance using highlights," *Image Vision Comput.*, vol. 9, no. 5, pp. 333–337, 1991.
[13] S. Tominaga, "Surface identification using the dichromatic reflection model," *IEEE Trans. Pattern Anal. Machine Intell.*, vol. 13, pp. 658–670, July 1991.
[14] B. V. Funt, M. S. Drew, and J. Ho, "Color constancy from mutual reflection," *Int. J. Comput. Vision*, vol. 6, pp. 5–24, Apr. 1991.
[15] M. Tsukada and Y. Ohta, "An approach to color constancy using multiple images," in *Proc. 3rd Int. Conf. Comput. Vision*, vol. 3, 1990, pp. 385–389.
[16] M. D'Zmura and G. Iverson, "Color constancy. I basic theory of two-stage linear recovery of spectral descriptions for lights and surfaces," *J. Opt. Soc. Amer. A*, vol. 10, no. 10, pp. 2148–2165, Oct. 1993.
[17] ——, "Color constancy. II results for two-stage linear recovery of spectral descriptions for lights and surfaces," *J. Opt. Soc. Amer. A*, vol. 10, no. 10, pp. 2166–2180, Oct. 1993.
[18] M. D'Zmura, G. Iverson, and B. Singer, "Probabilistic color constancy," in *Geometric Representations of Perceptual Phenomena*. Mahwah, NJ: Lawrence Erlbaum, 1995, pp. 187–202.
[19] S. Tominaga, "Multichannel vision system for estimating surface and illumination functions," *J. Opt. Soc. Amer. A*, vol. 13, no. 11, pp. 2163–2173, Nov. 1996.
[20] D. H. Brainard and W. T. Freeman, "Bayean color constancy," *J. Opt. Soc. Amer. A*, vol. 14, no. 7, pp. 1393–1411, July 1997.
[21] G. D. Finlayson, "Color in perspective," *IEEE Trans. Pattern Anal. Machine Intell.*, vol. 18, pp. 1034–1038, Oct. 1996.
[22] G. D. Finlayson, P. M. Hubel, and S. Hordley, "Color by correlation," in *Proc. 5th Color Imaging Conf.*, Springfield, VA, 1997, pp. 6–11.
[23] K. Barnard, L. Matin, and B. Funt, "Color by correlation in a three-dimensional color space," in *Proc. 6th Eur. Conf. Comput. Vision*, July 2000, pp. 275–289.
[24] G. Sapiro, "Color and illuminant voting," *IEEE Trans. Pattern Anal. Machine Intell.*, vol. 21, pp. 1210–1215, Nov. 1999.
[25] C. H. Lee, B. J. Moon, H. Y. Lee, E. Y. Chung, and Y. H. Ha, "Estimation of spectral distribution of scene illumination from a single image," *J. Imag. Sci. Technol.*, vol. 44, no. 4, pp. 308–320, 2000.
[26] M. H. Brill, "Image segmentation by object color: a unifying framework and connection to color constancy," *J. Opt. Soc. Amer. A*, vol. 7, no. 10, pp. 2041–2047, 1986.
[27] G. J. Klinker, S. A. Shafer, and T. Kanade, "Image segmentation and reflectance analysis through color," in *Proc. SPIE, Application of Artificial Intelligence VI*, vol. 937, 1988, pp. 229–244.
[28] R. Bajcsy, S. W. Lee, and A. Leonardis, "Color image segmentation with detection of highlights and local illumination induced by inter-reflection," in *Proc. Int. Conf. Pattern Recognition*, Atlantic City, NJ, 1990, pp. 785–790.
[29] G. Healey, "Segmenting images using normalized color," *IEEE Trans. Syst., Man, Cybern.*, vol. 22, pp. 64–73, Jan. 1992.
[30] R. Bajcsy, S. W. Lee, and A. Leonardis, "Detection of diffuse and specular interface reflections and inter-reflections by color image segmentation," *Int. J. Comput. Vision*, vol. 17, no. 3, pp. 241–272, 1996.
[31] S. Wesolkowski, S. Tominaga, and R. D. Dony, "Shading and highlight invariant color image segmentation using the mpc algorithm," in *Proc. SPIE, Color Imaging: Device-Independent Color, Color Hard Copy and Graphic Arts VI*, San Jose, CA, Jan. 2001, pp. 229–240.

[32] P. M. Hubel, J. Holm, and G. Finlayson, "Illuminant estimation and color correction," in *Color Imaging*. New York: Wiley, 1999, pp. 73–95.
[33] G. Sharma and H. J. Trussell, "Digital color imaging," *IEEE Trans. Image Processing*, vol. 6, pp. 901–932, July 1997.
[34] W. Wu and J. P. Allebach, "Imaging colorimetry using a digital camera," *J. Imag. Sci. Technol.*, vol. 44, no. 4, pp. 267–279, July/Aug. 2000.
[35] V. C. Cardei and B. Funt, "Color correcting uncalibrated digital camera," *J. Imag. Sci. Technol.*, vol. 44, no. 4, pp. 288–294, July/Aug. 2000.
[36] R. S. Berns, "Challenges for color science in multimedia imaging," in *Color Imaging*. New York: Wiley, 1999, pp. 99–128.
[37] L. W. MacDonald, "Color image engineering for multimedia systems," in *Color Imaging*. New York: Wiley, 1999, pp. 191–214.
[38] M. J. Swain and D. H. Ballard, "Color indexing," *Int. J. Comput. Vision*, vol. 7, no. 1, pp. 11–32, 1991.
[39] B. V. Funt and G. Finlayson, "Color constant color indexing," *IEEE Trans. Pattern Anal. Machine Intell.*, vol. 17, pp. 522–529, May 1995.
[40] M. S. Drew, J. Wei, and Z. N. Li, "Illumination-invariant image retrieval and video segmentation," *Pattern Recognit.*, vol. 32, no. 8, pp. 1369–1388, 1999.
[41] R. Schettini, G. Ciocca, and I. Gagliardi, "Content-based color image retrieval with relevance feedback," in *Proc. Int. Conf. Image Processing*, Oct. 1999, pp. 27AS2.8–27AS2.8.
[42] S. Tominaga, S. Ebisui, and B. A. Wandell, "Color temperature estimation of scene illumination," in *Proc. 7th Color Imaging Conf.*, Nov. 1999, pp. 42–47.
[43] ——, "Scene illuminant classification: Brighter is better," *J. Opt. Soc. Amer. A*, vol. 18, no. 1, pp. 55–64, 2001.
[44] G. Wyszecki and W. S. Stiles, *Color Science: Concepts and Methods, Quantitative Data and Formulae*. New York: Wiley, 1982.
[45] C. S. McCamy, "Correlated color temperature as an explicit function of chromaticity coordinates," *Color Res. Appl.*, vol. 17, pp. 142–144, 1992.
[46] D. B. Judd, "Sensibility to color-temperature change as a function of temperature," *J. Opt. Soc. Amer.*, vol. 23, pp. 127–134, 1933.
[47] M. J. Vrhel, R. Gershon, and L. S. Iwan, "Measurement and analysis of object reflectance spectra," *Color Res. Appl.*, vol. 19, no. 1, pp. 4–9, Feb. 1994.
[48] [Online]. Available: http://www.osakac.ac.jp/labs/shoji

Shoji Tominaga (Senior Member, IEEE) was born in Hyogo Prefecture, Japan, on April 12, 1947. He received the B.E., M.S., and Ph.D. degrees in electrical engineering from Osaka University, Toyonaka, Osaka, Japan, in 1970, 1972, and 1975, respectively.

From 1975 to 1976, he was with the Electrotechnical Laboratory, Osaka, Japan. Since April 1976, he has been with Osaka Electro-Communication University, Neyagawa, Osaka, Japan, where he was a Professor with the Department of Precision Engineering, Faculty of Engineering, from 1986 to 1995 and is currently a Professor with the Department of Engineering Informatics, Faculty of Information Science and Arts. During the 1987–1988 academic year, he was a Visiting Professor with the Department of Psychology, Stanford University, Stanford, CA. He founded a visual information research group with the Kansai section of the Information Processing Society. His current research interests include computational color vision, color image analysis, computer image rendering, and color management.

Dr. Tominaga is a member of the optical Society of America, IS&T, SPIE, and ACM.

Brian A. Wandell was born in New York, NY, on October 6, 1951. He received the B.S. degree in mathematics and psychology from the University of Michigan, Ann Arbor, in 1973 and the Ph.D. degree from the University of California, Irvine, in 1977.

He joined the Faculty of Stanford University in 1979. In engineering, he founded the Image Systems Engineering Program at Stanford. He is Co-Principal Investigator of the Programmable Digital Camera program, an industry-sponsored effort to develop programmable CMOS sensors. He authored *Foundations of Vision* (Sunderland, MA: Sinauer, 1995), a textbook on vision science. His research includes the image systems engineering and vision science. His work in vision science uses both functional MRI and psychophysics and includes the computation and representation of color and measurements of reorganization of brain function during development and following brain injury.

Dr. Wandell is a Fellow of the Optical Society of America. He received the 1986 Troland Research Award from the U.S. National Academy of Sciences for his work in color vision, the McKnight Senior Investigator Award in 1997, and the Macbeth Prize from the Inter-Society Color Council in 2000.